Journal of Communications Technology and Electronics, Vol. 45, No. 6, 2000, pp. 664–669. Translated from Radiotekhnika i Elektronika, Vol. 45, No. 6, 2000, pp. 735–741.
Original Russian Text Copyright © 2000 by Fetisov, Patton.
English Translation Copyright © 2000 by MAIK "Nauka /Interperiodica" (Russia).

RADIO PHENOMENA IN SOLIDS AND PLASMA

Microwave Bistability in a Nonlinear Film Ferromagnetic Resonator

Yu. K. Fetisov and C. E. Patton

Received December 2, 1999

Abstract—Bistability inherent in the interaction of the microwave radiation and a film ferromagnetic resonator is experimentally investigated in the presence of ferromagnetic resonance. It is shown that the bistability is due to the resonator frequency shift and the intrinsic nonlinearity of the resonance observed at high amplitudes of the magnetization precession. Results of measurements are interpreted in terms of the dispersion–absorption model of bistability.

INTRODUCTION

When high-power microwave (MW) radiation interacts with ferrites in the presence of the ferromagnetic resonance (FMR), a number of nonlinear phenomena are observed which are caused by an abrupt increase in the amplitude of magnetization oscillations. Among these are the FMR saturation, generation of spin waves, frequency multiplication, and so on (see [1, 2] and references therein). These phenomena are of physical interest, and many of them are applied to MW electronic devices.

In this paper, we investigate the bistability inherent in the interaction of the MW radiation with the film ferromagnetic resonator. Recently, this phenomenon was discovered experimentally [3, 4]. It is shown that the bistability is due to the intrinsic FMR nonlinearity making the resonator frequency depend on power. As a result, the resonator may operate in one of the two stable states corresponding to the low or high absorbed (reflected) power. When the power of the fixed-frequency MW field exciting the resonator varies cyclically, one can observe a classic bistable hysteresis loop. A bistable FMR resonator can serve as a basis for creating various MW signal processing devices.

Until recently, bistability was mostly studied in optical nonlinear resonators [5] in order to design light-controlled optical elements. Among MW phenomena, the so-called foldover effect (i.e., the hysteresis dependence of the absorbed power on the magnetic field) observed in the presence of the FMR can be classified as the most similar to bistability. This effect was first predicted in 1955 [6] and was soon discovered experimentally [7] in ferrites. The foldover was observed at a fixed power incident on a ferrite sample in the presence of the cyclically varying intensity of a magnetic field. Various mechanisms causing the foldover in bulk and film samples were analyzed [7–12], including the intrinsic FMR nonlinearity and sample heating, which changes the saturation magnetization or ferrite anisotropy fields [13]. However, experimental data were not quantitatively compared to theoretical results for the foldover and, especially, for bistability. Therefore, contributions of different nonlinearity mechanisms to the formation of the nonlinear response of the FMR resonator and the possibility of calculating its characteristics are not analyzed. Note that the theory of the spin wave bistability in ferrite films was developed [14] and the existence of bistability in ferrite resonators was discussed [15].

A FERROMAGNETIC RESONATOR OPERATING AT A LOW POWER

In our measurements, a 4.9-μ-thick 1 × 1-mm yttrium iron garnet (YIG) ferrite film with the saturation magnetization $4\pi M_0 = 1750$ G was used as a ferromagnetic resonator. The film was grown on a [111] gadolinium gallium garnet substrate by liquid-phase epitaxy. The FMR in the film was excited by a 50-μm-wide 3-mm-long microstrip evaporated on the alumina substrate located near the film surface. The resonator–microstrip coupling was reduced by a 0.1-mm-thick dielectric layer inserted between the YIG film and alumina substrate. The structure was placed in the constant external magnetic field $H_0 = 3200$ Oe aligned with the normal to the film plane. As is shown below, this direction of the field provides optimal conditions for initiating the bistability. A monochromatic signal with the frequency f = 4–5 GHz and power P = –60 dBm–+20 dBm was applied to the microstrip from a MW generator through a circulator. A 70820A Hewlett-Packard panoramic analyzer was used to measure frequency spectra of the signal reflected from the resonator at a fixed signal power P and the reflected power P_r versus input power P at a fixed signal frequency f.

Figure 1 shows the frequency spectrum of the resonator measured at a low power, i.e., the reflection losses in decibels $L = 10\log(P_r/P)$ versus signal frequency f. The spectrum contains several absorption peaks: the main peak at 4170.3 MHz, a weaker peak at

4207.8 MHz, and a number of very weak peaks at higher frequencies. The spectrum does not change its form when the power incident on the resonator increases from –60 to –20 dBm, which indicates that the structure is linear at low signals.

The frequency spectrum of the resonator is formed due to forward bulk magnetostatic waves (FBMSWs) excited in the ferrite film whose characteristics are isotropic in the film plane. Using the familiar dispersion equation for FBMSWs in a normally magnetized film [16], taking into account the conditions providing standing waves due to reflection from the sample sides, and taking into consideration the demagnetization effect due to the finite dimensions of the resonator, one can obtain the following approximate expression for resonance frequencies of the rectangular resonator:

$$f_{nl} \simeq \gamma(H_0 - 4\pi M_z) + \gamma 4\pi M_z \frac{2d}{a} + \gamma 4\pi M_z \frac{\pi d}{4a}\sqrt{n^2 + l^2}. \quad (1)$$

The first term in (1) is the of the frequency of the uniform FMR in the infinite film magnetized along the normal to its surface, where H_0 is the intensity of the external field, M_z is the static component of the magnetization vector aligned with the field and perpendicular to the film plane, and $\gamma = 2.8$ MHz/Oe is the gyromagnetic ratio. At a low power, when angle θ of the magnetization vector precession around the field direction is small, component M_z is equal to ferrite saturation magnetization $M_z = M_0$. The second term in (1) gives the first-order correction to the frequency of the uniform FMR due to the finite ratio of ferrite film thickness d to film dimension a in the plane. The third term in (1) determines the frequency spectrum of the resonator, and the integer numbers $n = 1, 2, \ldots$ and $l = 1, 2$ correspond to different distributions of the high-frequency (HF) magnetization amplitude of standing waves along the length and across the width of the resonator.

In our experiment, the microstrip was located near the center of the ferrite sample parallel to its side. Therefore, it efficiently excited oscillations with $n = 1$ and $l = 1, 3, 5$ whose amplitudes had a maximum in the center of the resonator under the microstrip. The lower-order resonance frequencies calculated from (1) at the parameters used in the experiment are $f_{11} = 4134.7$ MHz and $f_{13} = 4167.6$ MHz. These values are in good agreement with the measured ones, and the difference between the adjacent resonance frequencies $f_{13} - f_{11} = 32.4$ MHz is also close to the measured value of 37.5 MHz. Slight differences between measured and calculated frequencies can be attributed to the effect of the field of the YIG crystal anisotropy and to nonuniformity of the internal magnetic field in the sample, which were neglected in our calculations and can be ignored in the subsequent analysis.

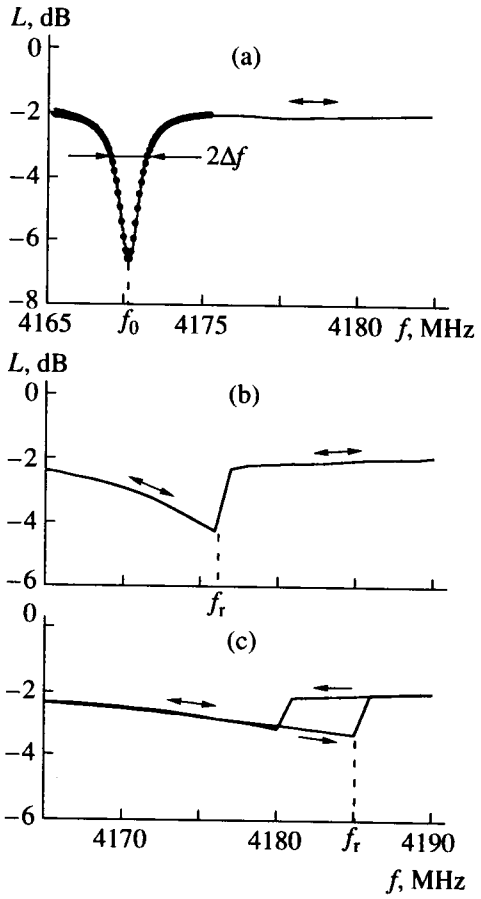

Fig. 1. Frequency spectrum of the FMR resonator (solid lines) measured and (dots) calculated at different signal powers: (a) –30, (b) 0, and (c) + 6 dBm; directions of signal frequency sweep are marked with arrows.

Figure 1a also shows that frequency-independent losses due to absorption in the circulator and cables of the measuring circuit are $L_0 = -1.9$ dB. The resonance losses at the central frequency of the main resonance $f_0 = f_{11} = 4170.3$ MHz are –4.5 dB, which yields the resonator MW power absorption factor $A_0 = P_a/P = 0.66$. The half-power width of the resonator absorption line is $2\Delta f = 2.0$ MHz. Dots in Fig. 1a mark the calculated absorption line of the described resonator, which is discussed below. In the following, we study the behavior of the main resonance at frequency f_0 versus power incident on the resonator.

CHARACTERISTICS OF THE RESONATOR OPERATING AT A HIGH POWER

Increasing signal power P from –20 to 0 dBm caused a nonlinear shift of resonance frequency f_r corresponding to the maximum absorption when the frequency is swept upwards and causes a nonsymmetrical

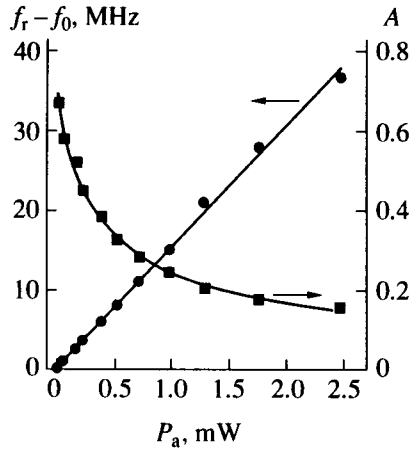

Fig. 2. Resonance frequency shift $f_r - f_0$ and absorption factor A of the resonator at frequency f_r vs. power P_a absorbed in the resonator: (dots) experiment and (solid lines) analytical approximation of the experimental data.

distortion of the line as shown in Fig. 1b. When the power was further increased from 0 to 20 dBm, the maximum shift of f_r reached 40 MHz and the hysteresis was observed in the frequency dependence of the resonator reflection losses (Fig. 1). When the signal frequency was increased from the minimum value, the reflected power first gradually decreased, next increased stepwise at $f = f_r$, and then was dependent of frequency. When the frequency was decreased from the maximum value, the reflected power remained constant until the frequency reached a certain value lower than f_r; then, the power decreased stepwise; and, only after that, it gradually increased following the curve which corresponds to the upward frequency sweep. This effect of the absorption line distortion and the hysteresis are similar to the foldover earlier observed in the YIG films [7], where the magnetic field was swept at a fixed signal frequency.

Figure 2 plots the shift of resonance frequency $f_r(P_a)$ and the resonator absorption factor $A(P_a) = P_a(f_r)/P$ at this frequency versus power P_a absorbed in the resonator. This figure shows the theoretical dependences and experimental ones obtained from measurements similar to those shown in Fig. 1. One can see that, when P_a varies from 0 to 2.5 mW (which corresponds to P varied from 0 to 17 mW), the resonance frequency of the resonator increases almost linearly with power at a rate $B = (15.2 \pm 0.6)$ MHz/mW, while the resonator absorption factor A monotonically decreases from 0.66 to 0.15.

Thus, the frequency measurements show that the resonator has a high Q-factor ($Q = f_0/2\Delta f \approx 2085$) at a low power and exhibits considerable nonlinearity causing a shift of the resonance frequency, which noticeably exceeds the line width. These properties of the resonator provide the existence of bistability.

BISTABILITY CHARACTERISTICS OF THE RESONATOR

Figure 3 shows typical dependences of reflected power P_r versus power P incident on the resonator measured at different fixed frequencies f of the continuous input signal. Note that function $P_r(P)$ was always linear when signal frequency f was smaller than the resonator low-power resonance frequency f_0. The nonlinearity was observed only when the signal frequency exceeded f_0.

When the initial signal frequency offset $\delta f = f - f_0$ exceeded $\delta f_{min} = 2.2$ MHz, the bistability region appeared in dependence $P_r(P)$. When the input signal power increased from zero, power P_r first linearly increased, next decreased stepwise at $P = P_1$, and then again monotonically increased. When the input signal power decreased from the maximum value, power P_r first monotonically decreased until $P = P_2$, where it increased stepwise and then, with the further decrease of input power P_r, followed the corresponding section of the curve for increasing power. Thus, when the signal power varied in the range $P_2 < P < P_1$, a particular input power was associated with either high or low reflected power P_r, depending on the previous history. The maximum difference between the high and low power levels was 2 dB. Figure 3 show that, as initial signal frequency offset δf increases, the bistability region moves towards higher input powers and its width increases.

Similar dependences $P_r(P)$ were measured at fixed frequencies in the pulsed mode with 1–10-μs pulses following at a 1-μs repetition period. In the pulsed mode, only a stepwise decrease of P_r was observed at $P = P_1$, while the bistability region was absent in dependences $P_r(P)$. The curves for increasing and decreasing P were identical and coincided with the similar dependence for increasing P in the continuous mode. The measured transition time between states with the high and low reflected power was $\tau \approx 2$ μs, which was of the same order of magnitude as the time interval during which steady-state oscillations are formed in the resonator with the width of the resonance curve $2\Delta f = 2$ MHz. When the power of excitation pulses is more than +18 dBm, the reflected pulse had a characteristic clipped flat top, which indicates parametric excitation of spin waves in the ferrite film. Thus, the results of pulse measurements demonstrate that the discovered bistability is due to the intrinsic FMR nonlinearity rather than to the heating of the ferrite sample caused by the MW power absorption.

MODEL OF DISPERSION–ABSORPTION BISTABILITY

In order to study the mechanism forming the MW bistability, we modify the phenomenological model of the dispersion bistability developed in optics [17] and apply it to the film FMR resonator.

At a low power level, the absorption line of the FMR resonator is described by the Lorentz expression

$$P_a(f) = P\frac{A}{1+\{(f-f_r)/\Delta f\}^2}, \quad (2)$$

where one must set $f_r = f_0$ and $A = A_0$ as $P \longrightarrow 0$. Then, the reflection losses (measured in decibels) of the resonator as a function of frequency are determined by the formula $L(f) = L_0 + 10\log\{1 - P_a(f)/P\}$, where P_a is expressed by (2) and, as mentioned above, L_0 (equal to −1.9 dB) gives the nonresonance signal losses in the measuring circuit. From Fig. 1a, one can see that the resonance curve calculated by this method adequately describes the absorption line of the resonator at the parameters used in the experiment.

As the signal power incident on the resonator increases, its resonance frequency shifts. As the experiment shows, this shift is due to the intrinsic FMR nonlinearity. Indeed, formula (1) shows that the resonator frequency strongly depends on static component M_z (perpendicular to the film plane) of the magnetization vector, the highest contribution being provided by the first term. As the MW signal power increases, angle θ of the magnetization vector precession around the field direction grows and, hence, M_z decreases. Taking into account that magnetization vector M_0 remains constant, we obtain that, in the first-order approximation, $M_z = M_0 - 2m^2/M_0$. Since squared amplitude m^2 of the HF magnetization is proportional to absorbed power P_a, equation (1) implies a linear increase of resonance frequency f_r with P_a, which is observed experimentally.

The resonance frequency of the resonator as a function of the absorbed power can be represented in the form

$$f_r = f_0 + BP_a, \quad (3)$$

where we use the frequency shift factor B = 15.2 MHz/mW found experimentally. For further calculations, we approximate experimental resonator absorption factor $A(P_a)$ versus the MW power by the analytic expression

$$A(P_a) = \frac{A_0}{0.83 + 1.85(P_a + 0.03)^{4/3}}, \quad (4)$$

where $A_0 = 0.66$ is the absorption factor of the resonator at $P_a \longrightarrow 0$ and P_a is given in milliwatts.

Substituting (3) and (4) into (1) yields P as an analytic function of P_a. Using this result, we can calculate power P_a absorbed in the resonator versus incident power P at a fixed signal frequency f.

Figure 4 shows typical dependences $P_a(P)$ calculated by this technique at the parameters used in the experiment. Straight line *1* demonstrates a linear dependence between the incident and absorbed powers $P_a = A_0P$ at resonance frequency f_0 in the absence of nonlinearity $B = 0$. Curves *2* and *3* are calculated for the resonator with the nonlinearity factor B = 15.2 MHz/mW. Curve *2* corresponds to the threshold initial frequency offset δf_{th} = 1.73 MHz, when a vertical

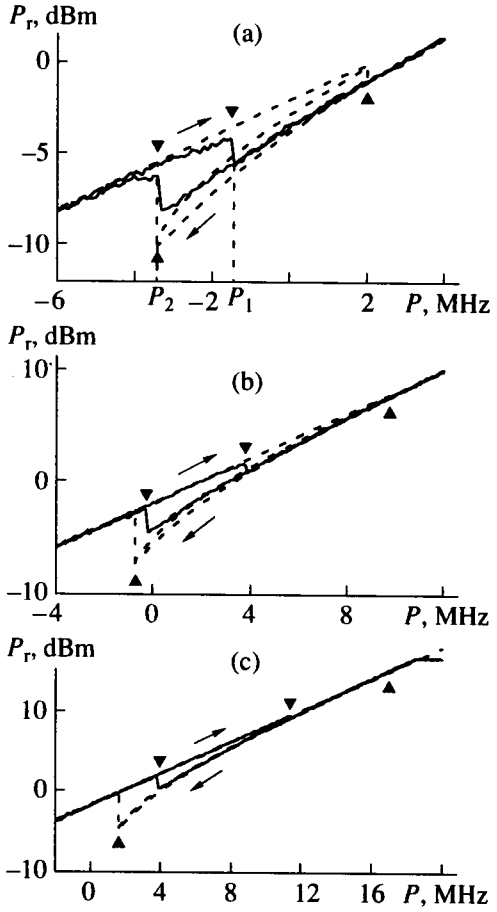

Fig. 3. Power P_r reflected from the resonator vs. incident power P (solid lines) measured and (dashed lines) calculated for the signal frequency offset δf = (a) 4.6, (b) 8.5 (b), and (c) 14.2 MHz. Directions of the increase or decrease of the incident power are marked with arrows. The boundaries of measured and calculated bistability loops are marked with triangles oriented, respectively, downwards and upwards.

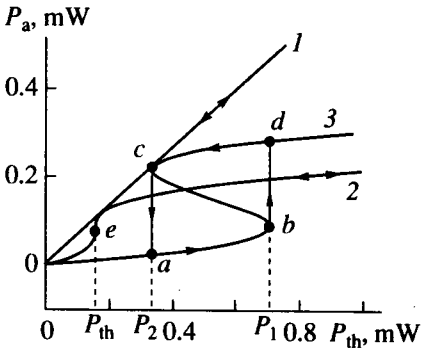

Fig. 4. Absorbed power P_a vs. incident power P calculated in (*1*) linear, (*2*) critical, and (*3*) bistability modes.

section with $\partial P/\partial P_a = 0$ appears in dependence $P_a(P)$. The threshold power at this point is denoted as P_{th}. A further increase of the initial signal frequency offset (curve *3* corresponds to $\delta f_{th} = 3.46$ MHz) produces the instability region between points *b* and *c*, where the absorbed power decreases with increasing input power. When P increases, power P_a first increases along curve *3*, then abruptly increases at $P = P_1$ from its value at point *b* to the value at point *d*, and again monotonically increases. When P decreases from the maximum value, P_a first monotonically decreases, passes point *d*, drops abruptly at $P = P_2$ from the value at point *c* to the one at point *a*, and then continues to decrease. Thus, when the input power varies in the range $P_2 < P < P_1$, the resonator exhibits bistability: a low or high (depending on the history) power absorbed in the resonator may correspond to a particular power incident on the resonator.

Conditions necessary for the bistability to occur in the resonator with the Lorentz absorption line can be expressed in an analytic form assuming that, at low-level signals, the absorption ratio of the resonator does not depend on the absorbed power and is equal to its initial value A_0. Then, using (2), (3), and the conditions that $\partial P/\partial P_a = 0$ and $\partial^2 P/\partial P_a^2 = 0$ at inflection point *e* (curve *2*, Fig. 4), we obtain the following inequalities after differentiation:

$$\delta f > \delta f_{th} = \sqrt{3}\Delta f, \quad P > P_{th} = \frac{8}{3\sqrt{3}}\frac{\Delta f}{A_0 B}. \qquad (5)$$

Hence, for the bistability to occur in the ferromagnetic resonator with the Lorentz absorption line, the initial frequency offset must exceed threshold value δf_{th}. In order to reduce the threshold power, the resonator must have a narrow absorption line, an absorption factor close to unity, and high nonlinearity. A decrease in the absorption factor of the resonator with the increasing power, which is typical of the nonlinear FMR, causes a certain increase in bistability threshold power P_{th}.

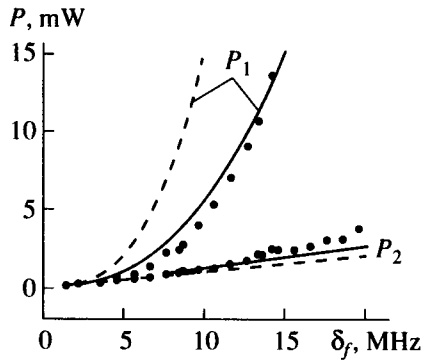

Fig. 5. Upper P_1 and lower P_2 boundaries of the bistability region in the YIG resonator vs. initial signal frequency offset: (dots) experiment, (dashed lines) calculations, and (solid lines) calculations taking into account the line broadening.

COMPARISON OF EXPERIMENTAL DATA WITH CALCULATIONS

In order to evaluate the applicability of the presented bistability model, we quantitatively compare measured and calculated data. In the experiment, bistability was observed when the minimum frequency mismatch and minimum power of the excitation MW signal were $\delta f_{min} = 2.2$ MHz and $P_{min} \approx 0.2$ mW, respectively, which is in good agreement with $\delta f_{min} = 1.73$ MHz and $P_{th} = 0.154$ mW calculated by (5) at the parameters used in the experiment.

Dashed lines in Fig. 3 plot the bistability loops of the resonator calculated at initial frequency offset δf used in the experiment. Calculations are performed by the above technique involving formulas (2)–(4) and the relationship for the reflected power $P_r = P - P_a$, by accounting for losses in the measuring circuit, and by using the parameters found from low-power measurements. In all of the three cases, the theory provides a good qualitative description of the shape and location of the bistability loops. However, the observed loop is smaller than the one predicted theoretically. Measured and calculated characteristic powers P_2 and, especially, P_1, at which the reflected power varies in a stepwise manner, substantially differ.

Figure 5 compares measured and calculated characteristic powers P_1 and P_2 versus initial frequency offset δf. The experimental points are obtained using measured data similar to those shown in Fig. 3. The theoretical curves (dashed lines) are calculated by the technique described above. One can see that, for any frequency offset, the observed bistability loop is more narrow than the loop predicted theoretically and is located within the calculated power interval. The greatest difference is observed in the calculated and measured values of upper boundary P_1 of the bistability loop at high frequency offsets corresponding to a high MW power incident on the resonator. The difference between the experimental and calculated data may be caused by the parametric excitation of spin waves at high amplitudes of the magnetization precession in the ferrite. It was demonstrated [1, 2] that, when the incident signal power is increased over a certain threshold value in an arrangement with the perpendicular pumping (as in our case), the energy is transferred from the uniform magnetization precession to the exchange spin waves. This effect manifests itself in the FMR absorption saturation, a more rapid decrease of longitudinal magnetization component M_z, and a broadening of the resonance curve with increasing MW power. In the case under consideration, first the absorption factor of the resonator decreases as shown in Fig. 2. Second, the estimate $\theta \sim \mathrm{Arccos}(M_z/M_0)$ of the magnetization precession angle corresponding to the maximum FMR fre-

quency shift of about 40 MHz yields $\theta \sim 7°$. This value significantly exceeds the limit angle $\theta_{spin} \sim 1°$, at which the parametric excitation of spin waves starts in the ferrite. Consideration of the FMR line broadening with increasing power provides a better agreement between the theory and experiment. This is illustrated by Fig. 5, which shows powers P_1 and P_2 (solid lines) versus initial frequency offset δf. These dependences are calculated by the above technique but using the expression $\Delta f(P_a) = \Delta f_0 + DP_a^2$ for the line width, where $\Delta f_0 = 1.0$ MHz and the only matching parameter $D = 60$ MHz/(mW)^2 is chosen so as to provide the best coincidence of calculated and measured powers.

Thus, the comparison of measured and calculated characteristics of the nonlinear film FMR resonator demonstrates that the phenomenological model of the dispersion–absorption bistability enables one to estimate the bistability characteristics of the resonator. However, in order to improve the agreement between calculated and experimental data, a theory should be developed that takes into account the parametric excitation of spin waves at high-level signals.

Bistable FMR resonators can be applied to processing and forming MW signals. As mentioned above, a low- or high-level reflected power corresponds to a particular input power in the bistability mode. Hence, applying an additional inphase or counterphase pulse signal of the appropriate amplitude to the input, one can switch the power of the reflected signal. Therefore, the resonator can be used as an MW power modulator directly controlled by another MW signal. A proper choice of resonator parameters and initial frequency offset can place it into the mode in which the reflected power slightly varies with a considerable variation of the incident power; i.e., the resonator operates as an MW power limiter. When the frequency offset of the resonator is slightly smaller than the threshold value necessary for initiating the bistability and a continuous bias signal (whose power is also close to the threshold value) is applied to the resonator input, small harmonic variations of the input power cause considerable variations of the output power, which can be regarded as the operation as an MW transistor. Bistable resonators switched from one stable state to another by an MW signal can be used as elements of logic MW devices.

CONCLUSION

It is found experimentally that, when MW radiation interacts with the FMR resonator in the form of a YIG ferrite film magnetized in the normal direction, bistability is observed when the offset between the signal and resonator frequencies at a low power and the power of the input signal exceed their threshold values. A cyclic variation of the signal power produces a characteristic bistability loop. The time interval during which the resonator is switched from one stable state to another is about several microseconds. Pulsed measurements demonstrate that the bistability is due to the intrinsic FMR nonlinearity rather than to the heating of the ferrite sample. The model of the dispersion–absorption bistability adequately describes characteristics of the bistable resonator. However, a theory taking into account the parametric excitation of spin waves in ferrite at a high power has to be developed in order to improve the quantitative coincidence of the calculated and measured results. FMR resonators can be applied as MW power limiters and modulators controlled by another MW signal and as MW logic elements.

ACKNOWLEDGMENTS

This work was supported in part by the National Science Foundation of the USA (grant nos. DMR-9400276 and DMR-9801649) and by the Ministry of Education of the Russian Federation.

REFERENCES

1. Monosov, Ya.A., *Nelineinyi ferromagnitnyi rezonans* (Nonlinear Ferromagnetic Resonance), Moscow: Nauka, 1971.
2. Gurevich A.G. and Melkov G.A., *Magnitnye kolebaniya i volny* (Magnetic Oscillations and Waves), Moscow: Nauka, 1994.
3. Fetisov, Yu.K. and Patton, C.E., *Tezisy dokladov XVI Mezhdunarodnoi shkoly-seminara "Novye magnitnye materialy mikroelektroniki"* (Abstracts of Papers of XVI International Workshop on New Magnetic Materials for Microelectronics), Moscow, 1998, Pt. 1, p. 276.
4. Fetisov, Y.K. and Patton, C.E., *Abstracts of Papers the 1998 MMM Conference. Miami, Florida. November 9–12*, 1998, p. 103.
5. Gibbs, H.M., *Optical Bistability. Controlling Light with Light*, New York: Academic, 1985.
6. Anderson, P.V. and Suhl, H., *Phys. Rev.*, 1955, vol. 100, no. 5, p. 1788.
7. Weiss, M.T., *Phys. Rev. Lett.*, 1958, vol. 1, no. 7, p. 239.
8. Skrotskii, G.V. and Alimov, Yu.A., *Zh. Eksp. Teor. Fiz.*, 1959, vol. 36, no. 9, p. 899.
9. Masters, J.I., *J. Appl. Phys.*, 1960, vol. 31, no. 1, p. 41S.
10. Seagle, D.J., Charap, S.H., and Artman, J.O., *J. Appl. Phys.*, 1985, vol. 57, no. 1, p. 3706.
11. McKinstry, K.D., Patton, C.E., and Kogekar, M., *J. Appl. Phys.*, 1985, vol. 58, no. 2, p. 925.
12. Gnatzig, K., Dotsch, H., Ye, M., *et al.*, *J. Appl. Phys.*, 1987, vol. 62, no. 12, p. 4839.
13. Zhang, Y.T., Patton, C.E., and Kogekar, M.V., *IEEE Trans. Magnetics*, 1986, vol. MAG22, no. 2, p. 993.
14. Bordman, A.D., Nikotov, S.A., and Wang, Q., *IEEE Trans. Magn.*, 1994, vol. MAG30, no. 1, p. 1.
15. Prabhakar, A. and Stancil, D.D., *J. Appl. Phys.*, 1999, vol. 85, no. 8, p. 4859.
16. Damon, R.W. and Van de Vaart, H., *J. Appl. Phys.*, 1965, vol. 36, no. 9, p. 3453.
17. Felberg, F.S. and Marburger, J.H., *Appl. Phys. Lett.*, 1976, vol. 28, no. 12, p. 731.